### Title
Controlling the Phase Transition in CsPbI3 Nanowires




### Journal
Nano Letters, 22(6)

### ISSN
1530-6984



### Authors
Lin, Chung-Kuan
Zhang, Ye
Gao, Mengyu
et al.



### Publication Date
2022-03-23

### DOI
10.1021/acs.nanolett.2c00170

Peer reviewed

# Controlling Phase Transition in $CsPbI_3$ Nanowires

Chung-Kuan Lin[1, 2+], Ye Zhang[1, 2+], Mengyu Gao[2, 3], Jia-An Lin[1], Han K. D. Le[1, 2], Zhenni Lin[2, 3], Peidong Yang[1, 2, 3, 4, *]

[1] Department of Chemistry, University of California Berkeley, Berkeley, California 94720, United States.

[2] Materials Sciences Division, Lawrence Berkeley National Laboratory, Berkeley, California 94720, United States.

[3] Department of Materials Science and Engineering, University of California Berkeley, Berkeley, California 94720, United States.

[4] Kavli Energy NanoScience Institute, Berkeley, California 94720, United States.

[+] These authors contributed equally to this work.

[*]Correspondence should be addressed to P.Y. (p_yang@berkeley.edu)

# Abstract

Cesium lead iodide ($CsPbI_3$) is a promising semiconductor with a suitable band gap for optoelectronic devices. $CsPbI_3$ has a metastable perovskite phase that undergoes phase transition into an unfavorable non-perovskite phase in ambient environment. This phase transition changes the optoelectronic properties of $CsPbI_3$ and hinders its potential for device applications. Therefore, it is of central importance to understand the kinetics of such instability and develop strategies to control and stabilize the perovskite phase. Here, we use ultralong $CsPbI_3$ nanowires as a model platform to investigate the phase transition kinetics. Our results depict the role of environmental stressors (moisture and temperature) in controlling the phase transition dynamics of $CsPbI_3$, which can serve as guiding principles for future phase transition studies and the design of related photovoltaics. Furthermore, we demonstrate the controllability of phase propagation on individual nanowires by varying moisture level and temperature.



# Keywords:

metal halide perovskites, single nanowire, phase transition, *in situ* imaging

# Introduction

Halide perovskites are a class of promising semiconductors that can be easily upscaled for use in optoelectronic devices, such as solar cells, lasers and light-emitting diodes,[1–5] and also model materials systems to investigate fundamental physical phenomena.[6–10] Among these phenomena, structural phase transition is particularly important, owing its relevance to the stability of perovskite-based devices.[4,7] Phase transition is a ubiquitous phenomenon in many kinds of solid-state materials, in which different phases exhibit distinctive properties due to their distinct crystal structures.[11,12] Halide perovskites exhibit diverse structural phases that undergo phase transition in response to environmental factors such as moisture or heat,[13–18] thus changing their optoelectronic properties and compromising their device stability. For example, the perovskite (high-temperature, HT) phase of all-inorganic cesium lead iodide ($CsPbI_3$) and cesium lead iodide/bromide alloy ($CsPbI_{3-x}Br_x$) are preferable for photovoltaic applications, but unfortunately metastable at room temperature, and they can transform into the non-perovskite (low-temperature, LT) phase upon exposure to moisture. This transition has led to the instability and poor device efficiency of their solar cells.[4,14] Thus, a mechanistic understanding of phase transition dynamics is needed to enable better phase control of the perovskite structure and higher stability of related photovoltaics.

A couple of studies have investigated this moisture-induced HT-to-LT phase transition behavior, as well as the reversible heat-driven LT-to-HT phase transition in inorganic halide perovskites.[6,18] Molecular dynamics (MD) simulations on the moisture-induced phase transition (MIPT) process reveals that a thin water layer adsorbed on the surface of HT-phase $CsPbI_3$ facilitates halide vacancy formation, which lowers the energy barrier to LT-phase nucleation.[14] Recent experiments demonstrate an exponential dependence of the phase nucleation rate as relative humidity (RH)

levels increase in the MIPT of $CsPbI_3$ microcrystals.[18] A phase transition involves two stages: phase nucleation and phase propagation (growth). Previous phase transition studies have not focused on propagation stage, possibly due to the geometry limitations of samples.[15,18] Propagation kinetics are also challenging to track; while polycrystalline thin films lack independence of grain boundary, nano- or microcrystal samples do not have a single, well-defined axial propagation direction, and phase transition events happen too fast in the small length scale of these materials. Therefore, the exploration of phase propagation kinetics necessitates a suitable material platform. Given the timescale of the growth kinetics (μm/sec), an ultralong (i.e. close to millimeter scale) nanowire (NW) form of HT-phase $CsPbI_3$ provides an ideal one-dimensional platform for analyzing phase propagation kinetics, owing to its well-defined interphase boundary along the axial direction and its length scale.[6] Furthermore, phase control on the single crystal level can be realized in the ultralong NW, and the phase transition process in inorganic halide perovskites can also be better visualized through *in situ* photoluminescence (PL) microscopy.

Here, we revealed the HT-to-LT phase transition kinetics on individual ultralong $CsPbI_3$ nanowires (NWs) and demonstrated controllable LT phase propagation at the single NW level by adjusting RH and temperature. The nucleation and propagation stages of the phase transition can be effectively separated on the millimeter-long NWs (grown on sapphire via chemical vapor transport). We observed that both, the nucleation fraction and the propagation rate increase with RH level (between 30% - 80% RH) and decrease with temperature (between 20°C- 50°C). With these ultralong $CsPbI_3$ NWs as a model platform, we then demonstrated that moisture and temperature can both serve as control knobs for tuning the phase propagation kinetics (i.e. accelerate or decelerate/stop) at the single NW level. Furthermore, with 350°C thermal heating

under inert environment, the LT phase can be driven back to HT phase again. This controllability can potentially provide solutions toward stabilizing the favorable HT phase for $CsPbI_3$-based photovoltaics, creating reconfigurable lattice on demand, and designing new heterostructures with tailorable optoelectronic properties.

## Results and Discussion

$CsPbI_3$ NWs on the M-plane sapphire substrates were prepared directly by chemical vapor transport (CVT) (see SI for more details).[19,20] We utilized a guided growth method that followed epitaxial and graphoepitaxial relationships between the material and substrate to guide the $CsPbI_3$ growth into well-aligned arrays. Due to the tiny accordion-like grooves on M-plane (10-10) sapphire, $CsPbI_3$ NWs can be guided to grow along the ± [11-20] directions of the sapphire structure.[19,20] The as-grown NWs had a large aspect ratio (around 1000), with a width around 1 μm and a length up to several millimeters (Figure 1c and S1). The scanning electron microscopy (SEM) images indicated that $CsPbI_3$ NWs had a triangular cross-section (Figure 1d and S1), with the height of the NW being about half of its width. Recently, Ernesto and coworkers have carried out a transmission electron microscopy (TEM) cross-section study on $CsPbBr_3$ NWs grown on M-plane (10-10) sapphire.[19–21] Due to the similar crystal structure, the $CsPbI_3$ NWs should grow along [001] direction despite a slightly different lattice size compared to $CsPbBr_3$. The chemical composition and distribution of the corresponding elements in $CsPbI_3$ NWs were confirmed by the energy-dispersive X-ray spectroscopy (EDS), showing that Cs, Pb, and I were uniformly distributed in the NW (Figure S2), with an atomic ratio of roughly 1:1:3. $CsPbI_3$ NWs grown with this CVT method adopted the HT perovskite phase, as confirmed by the PL emission centering at 710 nm (with a direct bandgap of ~ 1.73 eV) (Figure 1b).[22] As a metastable state in the ambient

environment, the HT phase of $CsPbI_3$ NWs undergoes transition into the LT phase upon exposure to moisture (schematic shown in Figure 1a).[18,23,24] The resulting LT phase of $CsPbI_3$ NWs had a much lower PL emission intensity, with a peak centering at 450 nm (Figure 1b). Raman spectroscopic measurement was carried out to identify the phase and the local symmetry unit. The measurement on HT NWs showed peaks from orthorhombic phase, while the measurement on LT NWs showed peaks from double-chain, non-perovskite phase on LT NWs (Figure S3).[25]

Rational control over the microstructure of a semiconductor is key to engineering its properties, and the ability to grow previously infeasible material geometries can often lead to new discoveries. This unique, ultralong NW platform has not only offered the opportunities to study epitaxial relationship between perovskite and the sapphire substrate,[19,20] but also enabled *in-situ* studies and the control of NW phase transition. With a propagation speed of less than a micrometer per second, the phase transition event in millimeter-long NWs would take minutes to complete, so the microscopic structural transformation could now be directly visualized in a practical timeframe. We used *in-situ* PL microscopy to capture the HT-to-LT phase transition kinetics on individual $CsPbI_3$ NWs under controlled RH and temperature conditions. The MIPT on ultralong $CsPbI_3$ NWs was observed to follow a similar reported mechanism,[14,18] containing the phase nucleation and growth stages. As time progressed, the HT-phase portions (red emission) gradually transformed into the LT-phase (blue emission) on each individual NW, as shown in Figure 2a. Here, we recorded the time evolution of phase transition events under different conditions to investigate the influence of environmental stressors (moisture and temperature). Substrates with arrays of $CsPbI_3$ NWs were consecutively placed in a closed chamber with different RH levels for experiments. A 650 nm light-emitting diode light (wide field) was employed to excite NWs, while

an optical microscope equipped with a charge-coupled device (CCD) camera was used to collect the PL emission. HT-phase $CsPbI_3$ can be distinguished from LT-phase $CsPbI_3$ by their different PL emission. Segments of fully transformed NWs turned from bright to completely dark, and this disappearance of bright emission was indicative of a phase transition event.

We analyzed the nucleation and propagation kinetics of the MIPT on these $CsPbI_3$ NWs separately. To make the comparison between different experiments meaningful, we compared the nucleation fraction of each measurement. Here we define the nucleation fraction as the number of nucleation events divided by the total number of NWs (chosen to be around 40 NWs), and this quantity can be tracked as time progresses. The nucleation of LT phase typically started from the ends of the NW with the appearance of the HT-LT phase interface, which can be distinguished by our wide-field fluorescence microscope (as shown in Figure 2a, 3a and video S1). We recorded the accumulated nucleation fractions versus time at different RH levels (38%, 53%, and 78%) and at a fixed temperature (room temperature, 22°C). As shown in Figure 2c and Figure S4, the nucleation fraction increased with the RH level. This increase can be explained by the fact that increasing RH provided a larger driving force for iodide ions to migrate toward the water layer on the surface, which increased the number of iodide vacancies on the surface of NW, leading to a reduction in energy barrier and a higher nucleation fraction.[14] The nucleation fraction versus RH level after 180 minutes was plotted in Figure 2b (left plot).

The dependence of phase nucleation on the temperature was also investigated. By controlling the temperature, the adsorbed surface water molecular coverage can be altered,[26,27] thus modulating the phase transition dynamics. As we increased the temperature from 22°C to 41°C (fixed RH level,

~55%), the nucleation fraction monotonically decreased with temperature (Figure 2d and Figure S5); the fraction at the end of 180 minutes is plotted on Figure 2b (right plot). Such dependence can be attributed to a decrease in the water layer coverage on the $CsPbI_3$ NW surface at elevated temperatures,[18] thus leading to a decrease in the halide vacancy concentration and an increase in nucleation energy barrier.[14,15] As a result, mild heating decelerated the LT phase nucleation of the MIPT in $CsPbI_3$.

The combination of the ultralong NW geometry and the high spatial resolution of PL imaging techniques allowed for a quantitative analysis of phase-propagation rates along the NW. Motivated by the uniqueness of this experimental platform, we designed experiments to investigate the dependence of the phase propagation rate on RH and temperature. After the LT phase nucleation was triggered on the NW, propagation of the LT phase proceeded along the axial direction of the NW (Figure 3a, right). We measured the propagation rate by tracking the distance that the HT-LT interface traveled within a time interval by using an *in-situ* PL microscopy. The propagation rate is defined as the distance that the interface travelled divided by the corresponding time interval. A clear HT-LT interface was also captured by SEM (Figure 3a, left). In the SEM image, the HT-phase portion of the NW showed a smooth surface (on the two exposed top planes), while the LT-phase portion showed crack formation, which can be explained by the relatively large change in the unit cell volume during the structural transformation from HT phase to LT phase.[28,29]

The RH- and temperature-dependent LT phase propagation rate is shown in Figures 3b and 3e, with each data point representing the average of propagation rates measured using 5 to 8 NWs. We observed that the propagation rate also increased with RH level when temperature was fixed at

22°C (Figure 3b, top). In principle, the phase growth kinetics can be described by an Arrhenius equation:

$$D = \nu \exp(-\frac{E_a}{K_B T})$$

where $D$ is the diffusion rate, ν is a frequency factor that contains atomic mobility, and $E_a$, $k_B$, and T represent the activation energy for propagation, the Boltzmann constant, and temperature, respectively.[6,30] The monotonic dependence of the phase-propagation rates on the RH levels indicated that the activation energy, $E_a$, was possibly dominated by moisture content (adsorbed on the $CsPbI_3$ surface). However, the activation energy for the phase growth could not be extracted from the temperature-dependent propagation measurement because higher temperature promoted water desorption that changed the phase energetics (i.e. $E_a$ is larger). As shown in Figure 3b (bottom), temperature played a counteracting role in the phase growth stage in our system; the average propagation rate decreased as the temperature increased (fixed RH level, RH~55%).

The aforementioned discussion and literature have mainly focused on the ensemble measurement under static thermodynamic conditions. How kinetic factors (*e.g.*, thermal fluctuation, dynamical moisture gradient) contribute to the phase transition trajectories on a single NW is an interesting topic, but is less explored. Here, our ultralong NWs provide a suitable platform for studying responses of phase propagation to dynamical environmental factors. For instance, one can track phase propagation while continuously changing external stressors (RH level and temperature). Therefore, instead of only measuring propagation under a static environment, as shown above (fixed RH and temperature), we changed the RH while the HT-LT interface was still propagating to observe the growth kinetics on a single NW *in situ* (experimental setup in Figure 3d). From a previous MD simulation, the characteristic timescale for the creation of one vacancy on the

perovskite surface was on the order of one millisecond,[14] and the propagation rate for NWs was on the order of 0.33 μm/s (at ambient condition, 23°C, RH=50%). Therefore, within 1 ms the HT-LT interface can only move about 0.33 nm. Comparing 0.33 nm with the millimeter total length of a NW, which is seven orders of magnitude longer, the interface can be considered as almost standing still. Further, water adsorption/desorption at a solid interface happens at a much faster time scale (ps to ns timescale),[31] therefore a change in the moisture level should have an instantaneous impact on the observed propagation rate. As shown in Figure 3c, the solid green lines indicate the distance travelled by the HT-LT interface on each NW within a time period (10 minutes). The propagation rate increased as we increased the RH level, demonstrating a similar trend and value as seen in ensemble measurement under static conditions (Figure 2b), and confirming that the change in RH level had a similar instantaneous effect on individual NWs. When the RH level was abruptly lowered, as exhibited in Figure 3e top column (between measurement number 4 and 5), the propagation was decelerated. We then gradually ramped up the RH level, at which point the propagation started to increase, showing that the acceleration and deceleration process was a "reversible" behavior (Figure 3e, between measurement 5-8). Here the "reversible" behavior refers to propagation rates being cycled/switched back and forth by tuning the environmental stressors.

Similar to the RH-dependent *in-situ* experiment, we conducted the *in-situ* temperature control experiments. A thermoelectric pad was placed underneath the NW sample, enabling us to precisely control the temperature (±1°C) by tuning the applied voltage. A K-type thermocouple was attached to the sample substrate for monitoring the temperature change; an infrared thermometer was employed to confirm the local temperature (Experimental schematic shown in Figure S6). When

the temperature was set at 23°C, the HT-LT interface on the NW propagated at a speed of 0.33 μm/s. When the temperature was increased to 50°C and held for a certain time (around 5 minutes), the propagation rate decreased significantly, approaching nearly 0.01 μm/s. When we reduced the temperature back to 23°C, a higher propagation rate was once again observed (at a speed of 0.33 μm/s) (Figure 4a), confirming a reversible behavior (RH fixed at 50%). We also carried out a cyclic temperature control experiment, measuring propagation rates as we continuously switched between different temperatures to further verify this reversibility (Figure 4b).

Thus far, we have shown that, by tuning the moisture level and temperature, one can effectively alter the propagation rate of an individual NW. The propagation behavior we observed was possibly due to a competition between the heating-facilitated atom diffusion and the heating-promoted water desorption on the NW surface. An earlier report from our group quantitatively described the detailed mechanism of the vacancy creation and activation energy reduction process due to water adsorption:[14] the number of vacancies increases exponentially with RH level, and the nucleation time (from HT to LT) decreases exponentially with vacancy concentration.[14] As previously mentioned, the water molecule adsorption and the vacancy creation processes are at a much faster timescale compared to the phase propagation in our ultralong NWs. Therefore, a change in moisture level should have an immediate impact on the observed propagation rate. Our experimental results suggested that this vacancy creation process was dynamic and reversible, and can be modulated at a single NW level. The vacancy creation process can be linked to the activation energy barrier reduction, as represented in Figure 4c (left: fewer vacancies; right: more vacancies) and Figure 4d. Furthermore, we demonstrated that heating the LT phase NWs at 350°C in an inert environment can drive the NW transition from LT to HT phase, and complete the entire phase

transition cycle (the NWs were quenched to room temperature after 350°C heating for 30 minutes, and afterwards they remained in metastable HT phase) (Figure S7). All of the above dynamic controls on the phase transition demonstrated the capability of designing and manipulating such a reconfigurable lattice on demand.

## Conclusion

In this work, we have investigated both the phase nucleation and propagation (growth) kinetics, from HT to LT in the MIPT of ultralong $CsPbI_3$ NWs. Our experiments revealed that both nucleation and propagation rate increase with RH and decrease with temperature. Utilizing moisture and heating as control knobs, we have demonstrated a reversible control on a single NW, where the propagation can be accelerated or decelerated down to the micrometer level. These dynamical and reversible controls stem from the enhancement or suppression of halide vacancy formation caused by water adsorption or desorption, thus effectively modulating the activation energy barrier of phase transition. Our results render new insights into the phase transition kinetics and offer strategy towards stabilizing the preferred HT phase of $CsPbI_3$, thus enabling applicability in perovskite solar cells and other optoelectronic devices. Further, this platform provides an ideal example of a reconfigurable lattice on demand and its tunability.

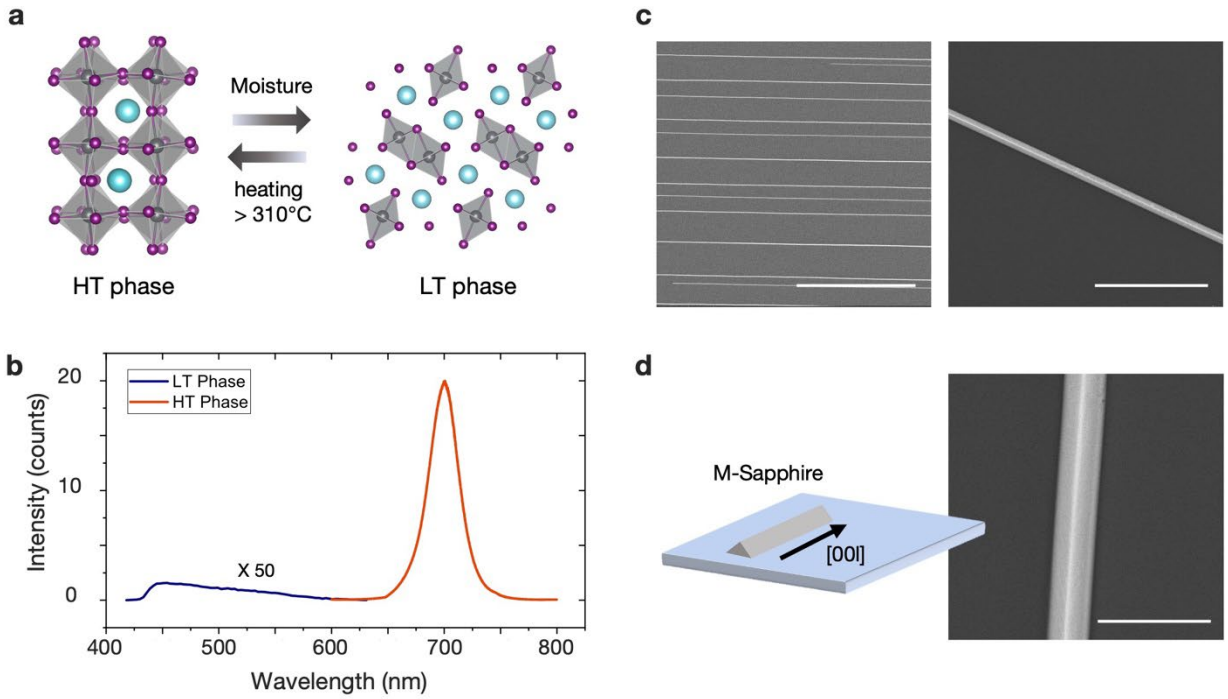


Figure 1. Characterization of $CsPbI_3$ NWs. (a) Schematic of the HT-$CsPbI_3$ and LT-$CsPbI_3$ phases. (b) PL spectra of HT and LT $CsPbI_3$ NWs. (c) SEM images of $CsPbI_3$ NWs on M-sapphire. Scale bar left: 25 μm. Scale bar right: 10 μm. (d) Left: Schematic illustration of the M-plane sapphire and directional growth of the NW. Right: Zoomed-in SEM image of the NW. Scale bar: 5 μm.

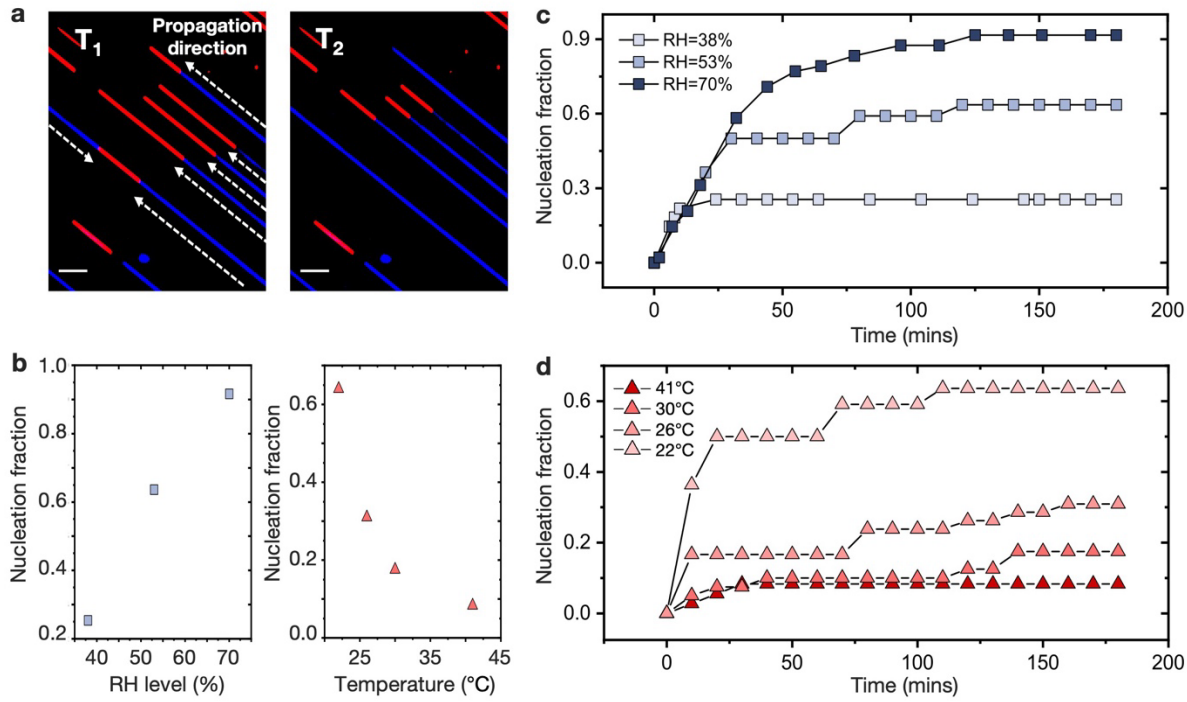


Figure 2. Nucleation behavior of $CsPbI_3$ NWs. (a) Representative confocal PL images illustrate nucleation behavior as time progresses (from $T_1$ to $T_2$). Red channel: 695-715 nm; Blue channel: 450-500 nm. Scale bar: 200 μm. (b) Left: Nucleation fraction at different RH levels (at 180 min). Right: Nucleation fraction at different temperatures (at 180 min). (c) Dependence of nucleation fraction to different RH. RH levels: 38%, 53% and 70%. (fixed temperature, ~22°C). (d) Dependence of the nucleation fraction to different temperatures. Temperatures: 22°C, 26°C, 30°C and 41°C. (fixed RH level, ~55%).

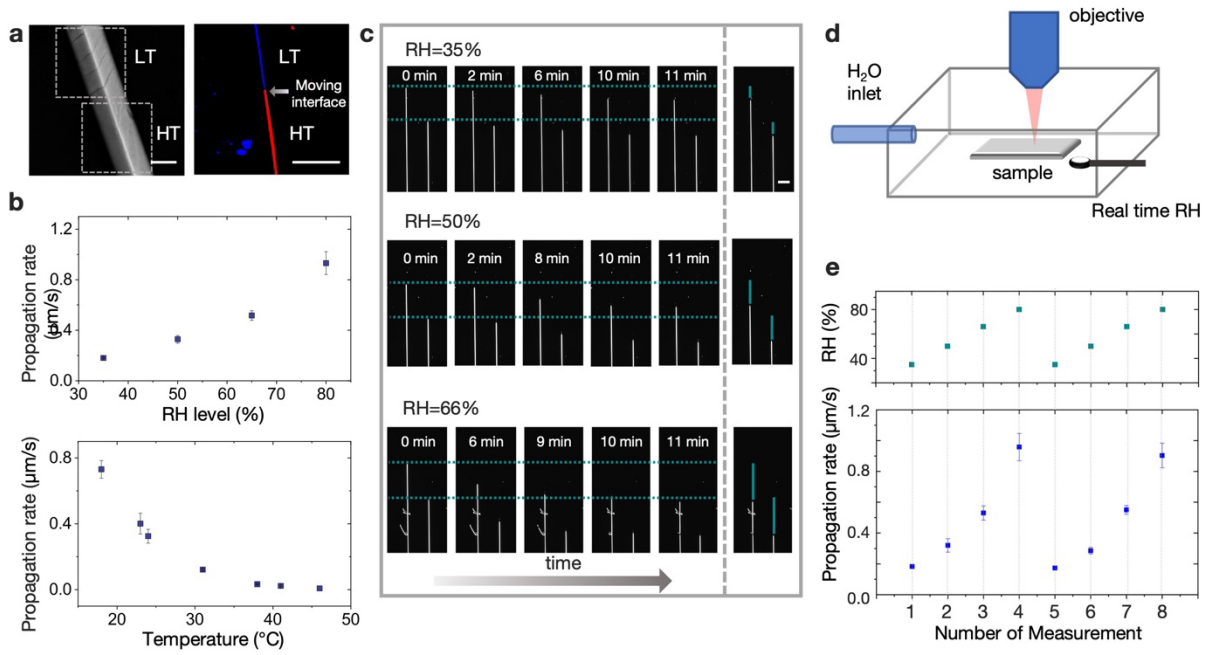


Figure 3. Propagation rate at static and dynamic conditions with moisture as a control knob for HT-LT propagation. (a) Left: SEM images of a HT-LT NW heterostructure. Scale bar: 1 μm. Right: Confocal PL images showing a moving interface between HT and LT phases. Red channel: 695-715 nm; Blue channel: 450-500 nm. Scale bar: 60 μm. (b) Top: Propagation rate at different RH level at fixed temperature (room temperature, ~22°C). Bottom: Propagation rate at different temperatures with a fixed RH level (RH~55%). (c) Time-lapse PL images of the NW under different RH levels. The dashed lines indicate the interface position in the beginning of the propagation; solid green lines mark the distance that interface has propagated within a time period (11 mins). Scale bar: 125 μm. (d) Experimental setup for in-situ RH control and read-out. (e) Propagation rate of the NW (lower plot) while dynamically changing the RH level (upper plot) (temperature fixed at 22°C).

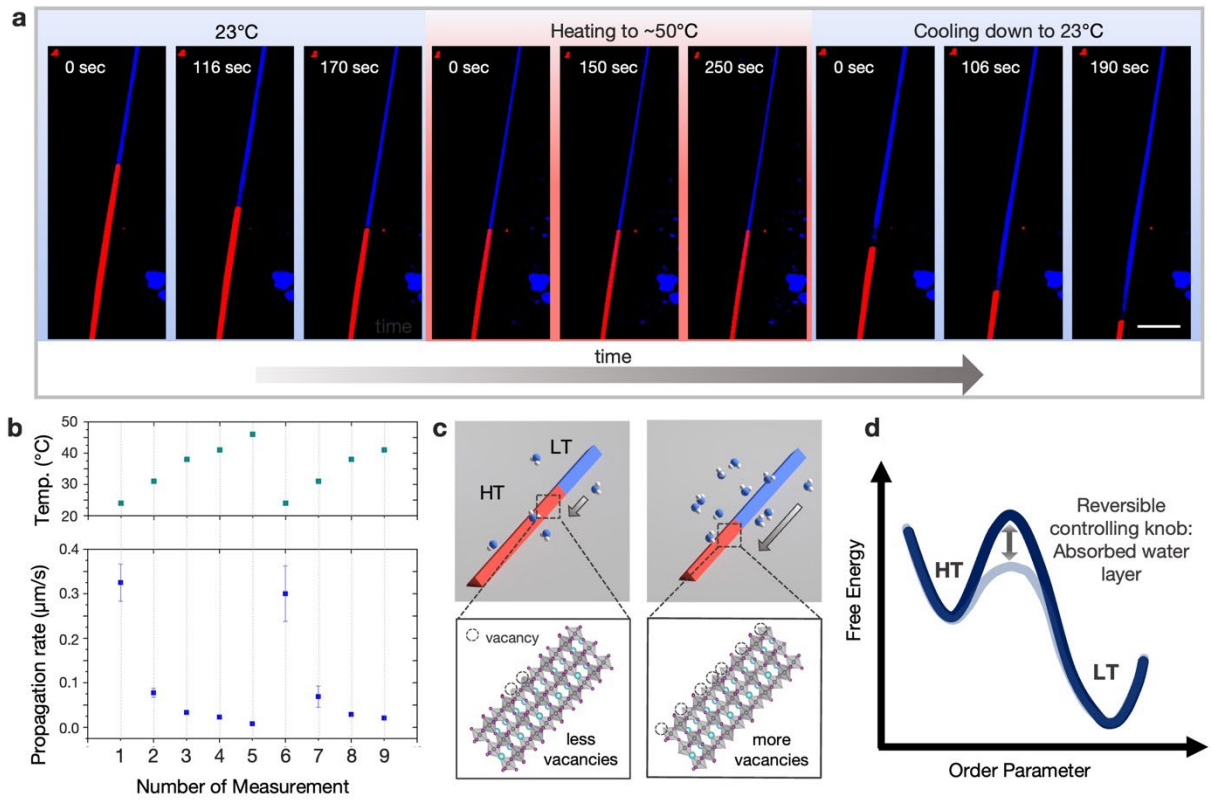


Figure 4. Temperature as a control knob for HT-LT propagation. (a) Time-lapse PL images of the NW. Scale bar: 35 μm. (b) Propagation rate of the NW (lower plot) while dynamically changing the temperature (upper plot) (RH fixed at 50%). (c) Schematics of the thin water molecule layer interacting with $CsPbI_3$ NW surface. (Left) fewer water molecules on the HT surface results in fewer surface halide vacancies compared to (right) more water molecule on the HT surface. (d) Schematic diagram showing moisture and temperature as control knobs to reversibly modulate the crystal phase between the metastable HT and the stable LT state.

# Supporting Information

The Supporting Information (PDF File) is available free of charge on the ACS Publications website.

Full description of NW synthesis, materials characterizations, SEM images and optical images of the ultralong NWs, EDS analysis for $CsPbI_3$ NWs, Raman spectrum on $CsPbI_3$ NWs, Time-lapsed PL images of nucleation at different conditions, Confocal PL images of LT-HT transition. A video showing NW phase propagation is also provided.

# Author Information

*Correspondence should be addressed to P.Y. (p_yang@berkeley.edu)

## Author Contributions

[+] These authors contributed equally to this work. C.K.L. and P.Y. designed the experiments. C.K.L carried out the in-situ optical characterizations, PL and Raman spectroscopy, SEM, SEM-EDS and grew perovskite materials with the help from Y.Z.. M.G. and J.A.L help analyze the data. All authors discussed the results and revised the manuscript. P.Y. supervised the project.

## Funding Sources

(1) US Department of Energy, Office of Science, Office of Basic Energy Sciences, Materials Sciences and Engineering Division, under Contract DE-AC02-05CH11231 within the Physical Chemistry of Inorganic Nanostructures Program (KC3103)

(2) Confocal laser scanning microscopic study was conducted at the College of Natural Resources Biological Imaging Facility, supported in part by the National Institutes of Health S10 Program under Award 1S10RR026866-01

## Acknowledgements

We thank P. Zhang, Siqi Wang and Renjie Tao for the help on PL and Raman measurements. We would like to thank Qiuchen Zhao for very helpful discussion during the manuscript preparation. We thank Alex Oddo for proofreading the manuscript. This work was supported by the US Department of Energy, Office of Science, Office of Basic Energy Sciences, Materials Sciences and Engineering Division, under contract DE-AC02-05CH11231 within the Physical Chemistry of Inorganic Nanostructures Program (KC3103). Confocal laser scanning microscopic study was conducted at the College of Natural Resources Biological Imaging Facility, supported in part by the National Institutes of Health S10 Program under award 1S10RR026866-01. Chung-Kuan Lin acknowledges MOE Technologies Incubation Scholarship from Taiwan. Ye Zhang acknowledges the fellowship supports from Suzhou Industrial Park.

# Reference


(1) Lee Michael M.; Teuscher Joël; Miyasaka Tsutomu; Murakami Takurou N.; Snaith Henry J. Efficient Hybrid Solar Cells Based on Meso-Superstructured Organometal Halide Perovskites. *Science* **2012**, *338* (6107), 643–647. https://doi.org/10.1126/science.1228604.

(2) Zhang, Q.; Shang, Q.; Su, R.; Do, T. T. H.; Xiong, Q. Halide Perovskite Semiconductor Lasers: Materials, Cavity Design, and Low Threshold. *Nano Lett.* **2021**, *21* (5), 1903–1914. https://doi.org/10.1021/acs.nanolett.0c03593.

(3) Dong, H.; Zhang, C.; Liu, X.; Yao, J.; Zhao, Y. S. Materials Chemistry and Engineering in Metal Halide Perovskite Lasers. *Chem. Soc. Rev.* **2020**, *49* (3), 951–982. https://doi.org/10.1039/C9CS00598F.

(4) Wang Yong; Dar M. Ibrahim; Ono Luis K.; Zhang Taiyang; Kan Miao; Li Yawen; Zhang Lijun; Wang Xingtao; Yang Yingguo; Gao Xingyu; Qi Yabing; Grätzel Michael; Zhao Yixin. Thermodynamically Stabilized β-CsPbI3–Based Perovskite Solar Cells with Efficiencies >18%. *Science* **2019**, *365* (6453), 591–595. https://doi.org/10.1126/science.aav8680.

(5) Kim, Y.-H.; Kim, S.; Kakekhani, A.; Park, J.; Park, J.; Lee, Y.-H.; Xu, H.; Nagane, S.; Wexler, R. B.; Kim, D.-H.; Jo, S. H.; Martínez-Sarti, L.; Tan, P.; Sadhanala, A.; Park, G.-S.; Kim, Y.-W.; Hu, B.; Bolink, H. J.; Yoo, S.; Friend, R. H.; Rappe, A. M.; Lee, T.-W. Comprehensive Defect Suppression in Perovskite Nanocrystals for High-Efficiency Light-Emitting Diodes. *Nat. Photonics* **2021**, *15* (2), 148–155. https://doi.org/10.1038/s41566-020-00732-4.

(6) Bischak, C. G.; Lai, M.; Fan, Z.; Lu, D.; David, P.; Dong, D.; Chen, H.; Etman, A. S.; Lei, T.; Sun, J.; Grünwald, M.; Limmer, D. T.; Yang, P.; Ginsberg, N. S. Liquid-like Interfaces Mediate Structural Phase Transitions in Lead Halide Perovskites. *Matter* **2020**, *3* (2), 534–545. https://doi.org/10.1016/j.matt.2020.07.015.

(7) Quarti, C.; Mosconi, E.; Ball, J. M.; D'Innocenzo, V.; Tao, C.; Pathak, S.; Snaith, H. J.; Petrozza, A.; De Angelis, F. Structural and Optical Properties of Methylammonium Lead Iodide across the

Tetragonal to Cubic Phase Transition: Implications for Perovskite Solar Cells. *Energy Environ. Sci.* **2016**, *9* (1), 155–163. https://doi.org/10.1039/C5EE02925B.

(8) Su, R.; Ghosh, S.; Wang, J.; Liu, S.; Diederichs, C.; Liew, T. C. H.; Xiong, Q. Observation of Exciton Polariton Condensation in a Perovskite Lattice at Room Temperature. *Nat. Phys.* **2020**, *16* (3), 301–306. https://doi.org/10.1038/s41567-019-0764-5.

(9) Becker, M. A.; Vaxenburg, R.; Nedelcu, G.; Sercel, P. C.; Shabaev, A.; Mehl, M. J.; Michopoulos, J. G.; Lambrakos, S. G.; Bernstein, N.; Lyons, J. L.; Stöferle, T.; Mahrt, R. F.; Kovalenko, M. V.; Norris, D. J.; Rainò, G.; Efros, A. L. Bright Triplet Excitons in Caesium Lead Halide Perovskites. *Nature* **2018**, *553* (7687), 189–193. https://doi.org/10.1038/nature25147.

(10) Ha, S.-T.; Shen, C.; Zhang, J.; Xiong, Q. Laser Cooling of Organic–Inorganic Lead Halide Perovskites. *Nat. Photonics* **2016**, *10* (2), 115–121. https://doi.org/10.1038/nphoton.2015.243.

(11) Manser, J. S.; Christians, J. A.; Kamat, P. V. Intriguing Optoelectronic Properties of Metal Halide Perovskites. *Chem. Rev.* **2016**, *116* (21), 12956–13008. https://doi.org/10.1021/acs.chemrev.6b00136.

(12) Wang, Y.; Xiao, J.; Zhu, H.; Li, Y.; Alsaid, Y.; Fong, K. Y.; Zhou, Y.; Wang, S.; Shi, W.; Wang, Y.; Zettl, A.; Reed, E. J.; Zhang, X. Structural Phase Transition in Monolayer MoTe2 Driven by Electrostatic Doping. *Nature* **2017**, *550* (7677), 487–491. https://doi.org/10.1038/nature24043.

(13) Gao, M.; Zhang, Y.; Lin, Z.; Jin, J.; Folgueras, M. C.; Yang, P. The Making of a Reconfigurable Semiconductor with a Soft Ionic Lattice. *Matter* **2021**, *4* (12), 3874–3896. https://doi.org/10.1016/j.matt.2021.09.023.

(14) Lin, J.; Lai, M.; Dou, L.; Kley, C. S.; Chen, H.; Peng, F.; Sun, J.; Lu, D.; Hawks, S. A.; Xie, C.; Cui, F.; Alivisatos, A. P.; Limmer, D. T.; Yang, P. Thermochromic Halide Perovskite Solar Cells. *Nat. Mater.* **2018**, *17* (3), 261–267. https://doi.org/10.1038/s41563-017-0006-0.

(15) Dastidar, S.; Hawley, C. J.; Dillon, A. D.; Gutierrez-Perez, A. D.; Spanier, J. E.; Fafarman, A. T. Quantitative Phase-Change Thermodynamics and Metastability of Perovskite-Phase Cesium Lead Iodide. *J. Phys. Chem. Lett.* **2017**, *8* (6), 1278–1282. https://doi.org/10.1021/acs.jpclett.7b00134.

(16) Venkatesan, S.; Hao, F.; Kim, J.; Rong, Y.; Zhu, Z.; Liang, Y.; Bao, J.; Yao, Y. Moisture-Driven Phase Transition for Improved Perovskite Solar Cells with Reduced Trap-State Density. *Nano Res.* **2017**, *10* (4), 1413–1422. https://doi.org/10.1007/s12274-017-1515-5.

(17) Lai, M.; Obliger, A.; Lu, D.; Kley, C. S.; Bischak, C. G.; Kong, Q.; Lei, T.; Dou, L.; Ginsberg, N. S.; Limmer, D. T.; Yang, P. Intrinsic Anion Diffusivity in Lead Halide Perovskites Is Facilitated by a Soft Lattice. *Proc. Natl. Acad. Sci.* **2018**, *115* (47), 11929. https://doi.org/10.1073/pnas.1812718115.

(18) Lin, Z.; Zhang, Y.; Gao, M.; Steele, J. A.; Louisia, S.; Yu, S.; Quan, L. N.; Lin, C.-K.; Limmer, D. T.; Yang, P. Kinetics of Moisture-Induced Phase Transformation in Inorganic Halide Perovskite. *Matter* **2021**, *4* (7), 2392–2402. https://doi.org/10.1016/j.matt.2021.04.023.

(19) Oksenberg, E.; Sanders, E.; Popovitz-Biro, R.; Houben, L.; Joselevich, E. Surface-Guided CsPbBr3 Perovskite Nanowires on Flat and Faceted Sapphire with Size-Dependent Photoluminescence and Fast Photoconductive Response. *Nano Lett.* **2018**, *18* (1), 424–433. https://doi.org/10.1021/acs.nanolett.7b04310.

(20) Shoaib, M.; Zhang, X.; Wang, X.; Zhou, H.; Xu, T.; Wang, X.; Hu, X.; Liu, H.; Fan, X.; Zheng, W.; Yang, T.; Yang, S.; Zhang, Q.; Zhu, X.; Sun, L.; Pan, A. Directional Growth of Ultralong CsPbBr3 Perovskite Nanowires for High-Performance Photodetectors. *J. Am. Chem. Soc.* **2017**, *139* (44), 15592–15595. https://doi.org/10.1021/jacs.7b08818.

(21) Oksenberg, E.; Merdasa, A.; Houben, L.; Kaplan-Ashiri, I.; Rothman, A.; Scheblykin, I. G.; Unger, E. L.; Joselevich, E. Large Lattice Distortions and Size-Dependent Bandgap Modulation in Epitaxial Halide Perovskite Nanowires. *Nat. Commun.* **2020**, *11* (1), 489. https://doi.org/10.1038/s41467-020-14365-2.

(22) Lai, M.; Kong, Q.; Bischak, C. G.; Yu, Y.; Dou, L.; Eaton, S. W.; Ginsberg, N. S.; Yang, P. Structural, Optical, and Electrical Properties of Phase-Controlled Cesium Lead Iodide Nanowires. *Nano Res.* **2017**, *10* (4), 1107–1114. https://doi.org/10.1007/s12274-016-1415-0.

(23) Ke, F.; Wang, C.; Jia, C.; Wolf, N. R.; Yan, J.; Niu, S.; Devereaux, T. P.; Karunadasa, H. I.; Mao, W. L.; Lin, Y. Preserving a Robust CsPbI3 Perovskite Phase via Pressure-Directed Octahedral Tilt. *Nat. Commun.* **2021**, *12* (1), 461. https://doi.org/10.1038/s41467-020-20745-5.

(24) Steele Julian A.; Jin Handong; Dovgaliuk Iurii; Berger Robert F.; Braeckevelt Tom; Yuan Haifeng; Martin Cristina; Solano Eduardo; Lejaeghere Kurt; Rogge Sven M. J.; Notebaert Charlotte; Vandezande Wouter; Janssen Kris P. F.; Goderis Bart; Debroye Elke; Wang Ya-Kun; Dong Yitong; Ma Dongxin; Saidaminov Makhsud; Tan Hairen; Lu Zhenghong; Dyadkin Vadim; Chernyshov Dmitry; Van Speybroeck Veronique; Sargent Edward H.; Hofkens Johan; Roeffaers Maarten B. J. Thermal Unequilibrium of Strained Black CsPbI3 Thin Films. *Science* **2019**, *365* (6454), 679–684. https://doi.org/10.1126/science.aax3878.

(25) Yang, Y.; Robbins, J. P.; Ezeonu, L.; Ma, Y.; Sparta, N.; Kong, X.; Strauf, S.; Podkolzin, S. G.; Lee, S. S. Probing Lattice Vibrations of Stabilized CsPbI3 Polymorphs via Low-Frequency Raman Spectroscopy. *J. Mater. Chem. C* **2020**, *8* (26), 8896–8903. https://doi.org/10.1039/D0TC02123G.

(26) Barraclough, P. B.; Hall, P. G. The Adsorption of Water Vapour by Lithium Fluoride, Sodium Fluoride and Sodium Chloride. *Surf. Sci.* **1974**, *46* (2), 393–417. https://doi.org/10.1016/0039-6028(74)90316-1.

(27) Toribio, F.; Bellat, J. P.; Nguyen, P. H.; Dupont, M. Adsorption of Water Vapor by Poly(Styrenesulfonic Acid), Sodium Salt: Isothermal and Isobaric Adsorption Equilibria. *J. Colloid Interface Sci.* **2004**, *280* (2), 315–321. https://doi.org/10.1016/j.jcis.2004.08.009.

(28) Straus, D. B.; Guo, S.; Cava, R. J. Kinetically Stable Single Crystals of Perovskite-Phase CsPbI3. *J. Am. Chem. Soc.* **2019**, *141* (29), 11435–11439. https://doi.org/10.1021/jacs.9b06055.

(29) Trots, D. M.; Myagkota, S. V. High-Temperature Structural Evolution of Caesium and Rubidium Triiodoplumbates. *J. Phys. Chem. Solids* **2008**, *69* (10), 2520–2526. https://doi.org/10.1016/j.jpcs.2008.05.007.

(30) Ferrando, R. Chapter 6 - Nonequilibrium Phenomena in Nanoalloys: From Nucleation to Ageing. In *Frontiers of Nanoscience*; Ferrando, R., Ed.; Elsevier, 2016; Vol. 10, pp 185–228. https://doi.org/10.1016/B978-0-08-100212-4.00006-7.

(31) Lane, J. M. D.; Leung, K.; Thompson, A. P.; Cuneo, M. E. Water Desorption from Rapidly-Heated Metal Oxide Surfaces—First Principles, Molecular Dynamics, and the Temkin Isotherm. *J. Phys. Condens. Matter* **2018**, *30* (46), 465002. https://doi.org/10.1088/1361-648X/aae4af.